EMRIs in Fundamental Fields

Francisco Duque

Max Planck Institute for Gravitational Physics (Albert Einstein Institute) Am Mühlenberg 1, D-14476 Potsdam, Germany

Abstract

Lecture Proceedings in "New Horizons for Ψ": In these lectures we are going to use standard techniques from Black-Hole Perturbation Theory to understand what is the effect that the presence of a superradiant (scalar) cloud around a supermassive black hole has on the trajectory of a stellar-mass compact body around it. We will then use our results to assess if future GW observations can help probing ultralight fields using the inspiral stage of binary coalescences.

Contents

1 Introduction

These notes guide a 2-hour lecture on *Extreme-Mass-Ratio Inspirals (EMRIs) in Fundamental Fields* for the New Horizons for Ψ School & Workshop, hosted at Instituto Superior Tecnico, University of Lisbon, from 1–5 July 2024.

Let us start by dissecting our title. First, *what* are EMRIs? They are binary systems where a stellar-mass *secondary* compact body with mass m_p, orbits around a much more massive object, with mass M, such that their mass ratio $\epsilon = m_p/M \lesssim 10^{-4}$ (systems where $10^{-4} \lesssim \epsilon \lesssim 10^{-2}$ are known as *intermediate*-mass-ratios inspirals – IMRIs) [1]. And *where* can we find such systems? The obvious example is the center of a galaxy, where a population of compact objects like stars, neutrons stars, or stellar-mass black holes (BH) is dancing around a central supermassive BH (SMBH), with $M \gtrsim 10^5 M_\odot$ [2]. And *why* should we care about EMRIs? In 2035, the European Space Agency is going to launch the *Laser Interferometer Space Antenna* (LISA), a constellation of 3 satellites trailing the Earth, separated by 2.5×10^6 km, that will be operating as a gravitational-wave (GW) interferometer sensitive to mHz frequencies [3]. EMRIs complete $\sim 10^5$ orbital cycles while in the LISA frequency range and can stay in band for the full 4 years of the mission [1, 4, 5]. This allows to constrain the parameters of the system with a relative precision as small as 10^{-5} (check Tables $3.6 - 3.7$ in the LISA Definition Study Report [3]), which will allow for the most stringent tests to General Relativity (GR) and Relativistic Astrophysics ever made [6–8], representing an improvement of 10^4 orders of magnitude with respect to current ground-based detectors [9]. However, this large number of orbital cycles is also synonymous with extremely complex trajectories and waveforms, which represent one of the hardest challenges in modelling and data analysis for LISA [10,11]. The disparity of mass scales between the secondary and primary makes EMRIs intractable to be tackled by Numerical Relativity (although see Ref. [12] for substantial progresses on IMRIs). Instead, the *self-force* program aims to solve the EMRI two-body problem by expanding the Einstein's equations in the mass-ratio ϵ [13, 14]. For the purposes of LISA, this expansion will need to be carried up to order $\mathcal{O}(\epsilon^2)$ [11].

Moving to the second part of the title, *Fundamental Fields* are the common theme of the school. At this stage, you are probably already familiar with some of the reasons to study them. New (ultra)light bosonic fields appear naturally in several extensions of GR in a wide range of mass scales $m_\Psi \sim 10^{-6} - 10^{-23}\,\text{eV}$ and have been proposed as a dark matter (DM) candidate [15–20]. From a technical standpoint, they are the simplest extension of vacuum-GR one can consider, so there is an "agnostic" pedagogical aspect in their study. But there is also astrophysical motivation behind it. When the field's Compton wavelength $\lambda_c = 1/\mu = m_\Psi/\hbar$ is comparable to the BH size, i.e. $M\mu \lesssim 0.5$, the field can extract rotational energy from the BH via *superradiance* (the wave analogous of the Penrose process) and condensate into boson clouds with an hydrogen atom-like structure [21–30]. These clouds are non-spherical and if the field is real emit GWs which can appear as continuous monochromatic sources or as collective stochastic GW background. Ground-based GW detectors, like the LIGO-Virgo-Kagra collaboration, target stellar-mass BHs, which probe masses around $\mu \sim 10^{-13}\,\text{eV}$ [31–34]. On the other hand, the fields can form self-gravitating structures, known as boson stars or DM solitons, which describe well the core of DM halos when they are "*fuzzy*", i.e., their mass is $m_\Psi \sim 10^{-23} - 10^{-19}$ eV) [35–44]. In particular, in this mass range the de Broglie wavelength is $\gtrsim$ kpc, and thus the field exhibits wave-like behavior, which helps in solving some tensions of the canonical Λ-CDM model at "small" length scales, such as the *cuspy-halo* problem [45–47].

EMRIs are present in galactic centers and we should therefore consider the impact that the presence of a ultralight bosonic environment has on their trajectory and subsequent GW signature. Here, we will focus on the simplest system we can think of involving an EMRI and a bosonic environment: a circular inspiral around a non-rotating BH surrounded by a spherical (complex) scalar cloud. This problem has been solved in Refs. [48, 49] (where Ref. [49] draws heavily from [50, 51]). Refs. [52–55] also made several important contributions using techniques from Quantum Mechanics, which we will discuss at the end. Alongside the notes, there is a MATHEMATICA notebook with a derivation of the equations of motion and a (rudimentary) ODE solver. My main focus was trying to be pedagogical and ensure someone who is doing these computations for the the first time can follow, so the system we will study is not the most realistic one and the code I provide is not the most robust (do not be surprised if you start playing with the parameters and something breaks!). But I hope that you can understand this simpler case and build from the tools provided if you want to explore further. Finally, let me thank Richard Brito, Andrea Maselli and Rodrigo Vicente, whose codes I have used as an inspiration.

2 Theoretical Setup

2.1 Action

Our starting point is a minimally coupled *complex* scalar Ψ evolving on an asymptotically flat spacetime described by the action [we work in geometrized units $G = c = 1$ and use the metric signature $(-+++)$]

$$S = \int d^4x\sqrt{-g}\big(\tfrac{1}{16\pi}R - \tfrac{1}{2}\partial_\mu\Psi\partial^\mu\Psi^* - \tfrac{1}{2}V(\Psi^*\Psi) + \mathcal{L}^{\rm m}\big), \tag{1}$$

where R is the Ricci scalar, V is the self-interaction potential of the scalar field, and $\mathcal{L}^{\rm m}$ describes the matter sector, which interacts with the scalar only via the minimal coupling to the metric $g_{\mu\nu}$.

Exercise. Check that this theory has a global U(1) symmetry with associated Noether current and charge, respectively,

$$J^\mu_Q = 2g^{\mu\nu}{\rm Im}\left[\Psi^*\partial_\nu\Psi\right] \quad , \quad Q = \int d^3x\sqrt{-g}J^t_Q, \tag{2}$$

and that varying the action above gives you the Einstein-Klein-Gordon system

$$G_{\mu\nu} = 8\pi(T^\Psi_{\mu\nu} + T^{\rm m}_{\mu\nu}) \qquad , \qquad \Box_g\Psi = \frac{\partial V}{\partial|\Psi|^2}, \tag{3}$$

where $\Box_g \equiv \partial_\mu\left[\sqrt{-g}\,\partial^\mu\left(\cdot\right)\right]/\sqrt{-g}$, plus a set of equations for the matter sector. Here, $G_{\mu\nu}$ is the Einstein tensor and the energy-momentum tensors of the scalar and matter are

$$T^\Psi_{\mu\nu} = \nabla_{(\mu}\Psi^*\nabla_{\nu)}\Psi - \frac{g_{\mu\nu}}{2}(\nabla^\alpha\Psi^*\nabla_\alpha\Psi + V) \qquad , \qquad T^{\rm m}_{\mu\nu} = \frac{-2}{\sqrt{-g}}\left[\frac{\delta(\sqrt{-g}\,\mathcal{L}_{\rm m})}{\delta g^{\mu\nu}}\right]. \tag{4}$$

As mentioned above, the large mass-ratio of our setup makes it suitable for a perturbative scheme. We will model the secondary as point particle of mass m_p, whose Lagrangian density and energy-momentum tensor are

$$\mathcal{L}^{\rm m} = m_p\int d\tau\tfrac{1}{\sqrt{-g}}\,\delta^{(4)}\left[x - x_p(\tau)\right] \quad , \quad T^{\mu\nu}_{\rm m} = m_p\int d\tau\frac{1}{\sqrt{-g}}\delta^{(4)}\left[x - x_p(\tau)\right]\dot{x}^\mu_p\dot{x}^\nu_p\,, \tag{5}$$

where $x_p(\tau)$ is the particle worldline parameterized by its proper time τ. This point particle is sourcing perturbations to a background spacetime which solves the Einstein-Klein-Gordon system at 0-th order and will represent the primary BH and the scalar field distribution around it. We are interested in finding solutions to first-order in ϵ

$$g_{\mu\nu} = \widehat{g}_{\mu\nu} + \epsilon\,\delta g_{\mu\nu} + \mathcal{O}(\epsilon^2) \quad , \quad \Psi = \widehat{\Psi} + \epsilon\,\delta\Psi + \mathcal{O}(\epsilon^2)\,. \tag{6}$$

2.2 The background

We will focus on spherically-symmetric background spacetimes (we had to start somewhere... in the end we will briefly discuss on how to extend this for the rotating case), for which the line element in spherical coordinates and the background scalar field are

$$\mathrm{d}\widehat{s}^2 \equiv \widehat{g}_{\mu\nu}dx^\mu dx^\nu \approx -A(r)dt^2 + \frac{dr^2}{B(r)} + r^2(d\theta^2 + \sin^2\theta d\varphi^2) \quad , \quad \widehat{\Psi} \approx \Psi_0(r)e^{-i\omega t}\,. \tag{7}$$

In general, the field's frequency ω is a complex number obtained from solving the 0-th order Einstein-Klein-Gordon system with appropriate boundary conditions (ingoing at the primary BH horizon and regularity at large r). In fact, *no-hair* theorems prevent the existence of spherically symmetric static solutions, i.e. solutions where ${\rm Im}(\omega)\neq 0$. However, for sufficiently light fields, the accretion timescale, which is dictated by $\tau_{\rm acc}\sim 1/{\rm Im}(\omega)$, can be much larger than the observation/inspiral timescale of an EMRI. For DM solitons, whose mass is typically much larger than the BH mass – our own Milky Way has a supermassive BH with $2\times10^6\,M_\odot$ and core DM halo estimated to have $\sim 10^9\,M_\odot$ – the accretion timescale is [44]

$$\tau^{\rm soliton}_{\rm acc} \lesssim 10\left(\frac{10^{10}M_\odot}{M_\Psi}\right)^5\left(\frac{m_\Psi}{10^{-22}\,{\rm eV}}\right)^6\,{\rm Gyr}\,, \tag{8}$$

which can be bigger than the Hubble time ($\tau_{\rm Hubble} \sim 14 \times 10^{-1}\,{\rm Gyr}$). For boson clouds, whose mass is much smaller than the primary, the decay is exponential on timescales (for spherical configurations) [44]

$$\tau_{\rm acc}^{\rm cloud} \lesssim 5 \times 10^9 \left(\frac{10^8 M_\odot}{M_\Psi}\right)^5 \left(\frac{m_\Psi}{10^{-22}\,{\rm eV}}\right)^6 {\rm Gyr}\,. \tag{9}$$

Then, we will assume the EMRI is inspiralling, or we are observing it, on a timescale much shorter than this accretion timescale. In this limit, we can take $\mathrm{Im}(\omega) = 0$ (this approximation is also used in both Refs. [48, 49]). Recall also that in the case of superradiant clouds, their growth ends in a true bound state around Kerr, with $\mathrm{Re}(\omega) = m\Omega_{\rm H}$ and $\mathrm{Im}(\omega) = 0$, where $\Omega_{\rm H}$ is the horizon's angular velocity [29].

2.3 The perturbations

The spherically symmetry of our background spacetime implies that any linear perturbation can be decomposed into irreducible representations of SO(3). For scalars, this is the standard expansion in spherical harmonics $Y_{\ell m}(\theta, \varphi)$

$$\delta\Psi = \frac{1}{r}\sum_{\ell,m}\int d\sigma\, \delta\psi_+^{\ell m}(r)\, e^{-i(\omega+\sigma)t} Y_{\ell m}(\theta,\varphi) \quad , \quad \delta\Psi^* = \frac{1}{r}\sum_{\ell,m}\int d\sigma\, \delta\psi_-^{\ell m}(r)\, e^{-i(\omega-\sigma)t}\, Y_{\ell m}(\theta,\varphi)\,, \tag{10}$$

where $\sum_{\ell,m} \equiv \sum_{\ell=0}^{\infty}\sum_{m=-\ell}^{\ell}$ and we move to Fourier domain $t \to \sigma$. We treat $\delta\Psi$ and $\delta\Psi^*$ as independent variables because with this decomposition we obtain equations of motion independent of the coordinate time t. To leave our equations as general as possible before applying them to a particular system, we expand the scalar field potential and its first derivative as

$$V \approx \widehat{V} + \sum_{\ell,m}\int d\sigma \delta V^{\ell m}(r) e^{-i\sigma t} Y_{\ell m}(\theta,\varphi) \quad , \quad U \equiv \frac{\partial V}{\partial|\widehat{\Psi}|^2} \approx \widehat{U} + \sum_{\ell,m}\int d\sigma \delta U^{\ell m}(r) e^{-i\sigma t} Y_{\ell m}(\theta,\varphi)\,. \tag{11}$$

Analogously, gravitational perturbations $\delta g_{\mu\nu}$ can be expanded in a basis of ten tensor spherical harmonics (the number of independent components of a rank-2 symmetric tensor), which depending on how they transform under parity transformations $(\theta,\varphi) \to (\pi-\theta, \pi+\varphi)$, can be grouped into polar/electric/even (do not change) or axial/magnetic/odd type (pick a $-$ sign)

$$\boldsymbol{\delta g}^{\rm axial} = \sum_{\ell,m} \frac{\sqrt{2\ell(\ell+1)}}{r}\left[i\, h_1^{\ell m}\boldsymbol{c}_{\ell m} - h_0^{\ell m}\boldsymbol{c}_{\ell m}^0 + \frac{\sqrt{(\ell+2)(\ell-1)}}{2} h_2^{\ell m}\boldsymbol{d}_{\ell m}\right]\,, \tag{12}$$

$$\begin{aligned}\boldsymbol{\delta g}^{\rm polar} = &\sum_{\ell,m} A\, H_0^{\ell m}\boldsymbol{a}_{\ell m}^0 - i\sqrt{2}H_1^{\ell m}\boldsymbol{a}_{\ell m}^1 + \frac{1}{B}H_2^{\ell m}\boldsymbol{a}_{\ell m} + \sqrt{2}K^{\ell m}\boldsymbol{g}_{\ell m} \\ &+ \frac{\sqrt{2\ell\,(\ell+1)}}{r}\left(h_1^{(e)\ell m}\boldsymbol{b}_{\ell m}^1 - i h_0^{(e)\ell m}\boldsymbol{b}_{\ell m}^0\right) + \left(\sqrt{\frac{(\ell+2)(\ell+1)\ell(\ell-1)}{2}}\boldsymbol{f}_{\ell m} - \frac{\ell\,(\ell+1)}{\sqrt{2}}\boldsymbol{g}_{\ell m}\right) G^{\ell m}\,.\end{aligned} \tag{13}$$

Here, the mode perturbations $h_1^{\ell m}$, $h_0^{\ell m}$, ... are functions of only (t, r), while $\boldsymbol{a}_{\ell m}^0$, $\boldsymbol{a}_{\ell m}$, ... are the ten tensor spherical harmonics depending only on (θ,φ), whose explicit form can be found in Ref. [56] (or in page 17 of Ref. [57] and also in the MATHEMATICA notebook).

Exercise. Check (at least for some of them) that the tensor spherical harmonics are defined to be orthonormal on the 2-sphere

$$\left(\boldsymbol{r}^{\ell' m'}, \boldsymbol{s}^{\ell m}\right) = \int_{S^2} d\Omega \left(r_{\mu\nu}^{\ell' m'}\right)^* s_{\lambda\rho}^{\ell m}\, \eta^{\mu\lambda}\, \eta^{\nu\rho} = \delta_{rs}\delta_{\ell\ell'}\delta_{mm'}\,, \tag{14}$$

where $\eta_{\mu\nu} = \mathrm{diag}\left(-1, 1, r^2, r^2\sin^2\theta\right)$. The energy-momentum tensor of the particle can also be expanded in this basis

$$\boldsymbol{T}_p = \sum_{\ell,m} \mathcal{A}_{\ell m}^0\boldsymbol{a}_{\ell m}^0 + \mathcal{A}_{\ell m}^1\boldsymbol{a}_{\ell m}^1 + \mathcal{A}_{\ell m}\boldsymbol{a}_{\ell m} + \mathcal{B}_{\ell m}^0\boldsymbol{b}_{\ell m}^0 + \mathcal{B}_{\ell m}\boldsymbol{b}_{\ell m} + \mathcal{Q}_{\ell m}^0\boldsymbol{c}_{\ell m}^0 + \mathcal{Q}_{\ell m}\boldsymbol{c}_{\ell m} + \mathcal{D}_{\ell m}\boldsymbol{d}_{\ell m} + \mathcal{F}_{\ell m}\boldsymbol{f}_{\ell m} + \mathcal{G}_{\ell m}\boldsymbol{g}_{\ell m}\,.$$

For a given source the expansion coefficients can be obtained by projecting the energy-momentum tensor on the respective spherical harmonic, e.g., $\mathcal{A}_{\ell m}^0 = (\boldsymbol{a}_{\ell m}^0, \boldsymbol{T})$.

2.3.1 Point-Particle Source

Exercise. As mentioned, the secondary is treated as a point-particle with energy-momentum tensor given in Eq. (5), which in spherical coordinates can be rewritten as

$$T^{\mu\nu}_m = T^{\mu\nu}_p = \int d\sigma\, e^{-i\sigma t} \frac{m_p}{r^2 \sin\theta} \sqrt{\frac{B}{A}} \frac{dt_p}{d\tau} \frac{dx^\mu}{dt} \frac{dx^\nu}{dt} \times \delta\left[r - r_p(t)\right] \delta\left[\theta - \theta_p(t)\right] \delta\left[\varphi - \varphi_p(t)\right] .$$

At leading order in ϵ, the secondary follows geodesic motion in the background spacetime determined by $\widehat{g}_{\mu\nu}$. However, part of the orbital energy is dissipated via GWs and the scalar configuration. For small enough ϵ (like in EMRIs), the energy dissipated over one orbit is much smaller than the orbital energy, and the secondary evolves *adiabatically* over a succession of geodesics. In other words, the orbital phase evolves on a timescale much shorter than the timescale over which quantities characterizing the orbit change, like its energy and angular momentum. This is the basis of the *two-timescale expansion* in which much of the self-force theory is built [4,58], and this adiabatic *flow* of geodesics corresponds to first-order self-force [10]. Here, we will assume (quasi-)circular motion (again, we had to start with the simplest case) for which

$$r_p(t) = r_p \quad , \quad \theta_p(t) = \frac{\pi}{2} \quad , \quad \varphi_p(t) = \Omega_p t \quad , \tag{15}$$

where

$$\Omega_p = \sqrt{\frac{A'_p}{2r_p}} \quad , \quad A_p \equiv A(r_p) \,, \tag{16}$$

and the associated energy and angular momentum per unit rest mass are

$$E_p = A_p \frac{dt_p}{d\tau} = \frac{A_p}{\sqrt{A_p - r_p^2\Omega_p^2}} \quad , \quad L_p = r_p^2 \frac{d\varphi_p}{d\tau} = \frac{r_p^2 \Omega_p}{\sqrt{A_p - r_p^2\Omega_p^2}} \,. \tag{17}$$

Exercise. Check that with the prescription above for the orbital motion, the source-term coefficients appearing in Eq. (15) are

$$\begin{aligned}
&\mathcal{A}_{\ell m} = \mathcal{A}^{(1)}_{\ell m} = \mathcal{B}_{\ell m} = \mathcal{Q}_{\ell m} = 0 \quad , \quad \mathcal{A}^0_{\ell m} = m_p \frac{\sqrt{AB}}{r^2} E_p\, Y^\star_{\ell m}\left(\frac{\pi}{2}, 0\right) \delta_r\, \delta_\sigma \quad , \\
&\mathcal{B}^0_{\ell m} = i\, m_p \frac{\sqrt{AB}}{r^3\sqrt{(n+1)}} L_p\, \partial_\phi Y^\star_{\ell m}\Big|_{(\pi/2,0)} \delta_r\, \delta_\sigma \quad , \quad \mathcal{Q}^0_{\ell m} = -m_p \frac{\sqrt{AB}}{r^3\sqrt{(n+1)}} L_p\, \partial_\theta Y^\star_{\ell m}\Big|_{(\pi/2,0)} \delta_r\, \delta_\sigma \,, \\
&\mathcal{G}_{\ell m} = m_p \frac{\sqrt{AB}}{r^4\sqrt{2}} \frac{L_p^2}{E_p} Y^\star_{\ell m}\left(\frac{\pi}{2}, 0\right) \delta_r\, \delta_\sigma \quad , \quad \mathcal{D}_{\ell m} = i\, m_p \frac{\sqrt{AB}}{r^4\sqrt{2n(n+1)}} \frac{L_p^2}{E_p} \partial_{\theta\phi} Y^\star_{\ell m}\Big|_{(\pi/2,0)} \delta_r\, \delta_\sigma \quad , \\
&\mathcal{F}_{\ell m} = m_p \frac{\sqrt{AB}}{r^4 2\sqrt{2n(n+1)}} \frac{L_p^2}{E_p} \left(\partial_{\phi\phi} - \partial_{\theta\theta}\right) Y^\star_{\ell m}\Big|_{(\pi/2,0)} \delta_r\, \delta_\sigma
\end{aligned} \tag{18}$$

where

$$n = \ell(\ell+1)/2 - 1 \quad , \quad \delta_r = \delta(r - r_p) \quad , \quad \delta_\sigma = \delta(\sigma - m\Omega_p) \,. \tag{19}$$

You might immediately notice that for $\ell = 1$, the coefficients $\mathcal{D}_{\ell m}$ and $\mathcal{F}_{\ell m}$ appear to diverge... We will look into that more carefully in the next section.

2.3.2 Gauge-Invariance

GR is invariant under diffeomorphisms, which at the linear level can be translated in the gauge invariance

$$x^\mu \to x'^\mu = x^\mu + \epsilon\, \xi^\mu \quad , \quad \delta g_{\mu\nu} \to \delta g'_{\mu\nu} = \delta g_{\mu\nu} - 2\nabla_{(\mu}\xi_{\nu)} \quad , \quad \delta\Phi \to \delta\Psi' = \delta\Psi - \xi^\mu \partial_\mu \widehat{\Psi} \,, \tag{20}$$

where ξ^μ is the vector field generating the (infinitesimal) diffeomorphism; we can use its four components to impose some coefficients in the expansion of $\delta g_{\mu\nu}$ to vanish. Note that ξ^μ can also be expanded in its polar and axial components

$$\begin{aligned}
\xi^\mu_{\rm polar} &= \sum_{\ell,m} \big(-\frac{1}{A}\xi^{\ell m}_t, B\xi^{\ell m}_r, 0, 0\big) Y_{\ell m} + \frac{\xi^{\ell m}_\Omega}{r^2 \sin\theta} \left(0, 0, \sin\theta\, \partial_\theta Y_{\ell m}, \partial_\varphi Y_{\ell m}\right) , \\
\xi^\mu_{\rm axial} &= \sum_{\ell,m} \frac{\xi^{\ell m}_{\rm ax}}{r \sin\theta} \left(0, 0, \partial_\varphi Y_{\ell m}, -\sin\theta\, \partial_\theta Y_{\ell m}\right) ,
\end{aligned}$$

where the $\xi_t^{\ell m}$, $\xi_r^{\ell m}$, $\xi_\Omega^{\ell m}$, $\xi_{\rm ax}^{\ell m}$ are only functions of (t, r).

Exercise. Check that in terms of the tensor spherical harmonics

$$
\begin{aligned}
2\boldsymbol{\nabla}\boldsymbol{\xi} = {} & \left(2\partial_t\xi_t - A'B\xi_r\right)\boldsymbol{a}^0 - i\sqrt{2}\left(\partial_r\xi_t + \partial_t\xi_r - \frac{A'}{A}\xi_t\right)\boldsymbol{a}^1 + \left(2\partial_r\xi_r + \frac{B'}{B}\xi_r\right)\boldsymbol{a} \\
& - i\frac{\sqrt{2\ell\,(\ell+1)}}{r}\left(\xi_t + \partial_t\xi_\Omega\right)\boldsymbol{b}^0 + \frac{\sqrt{2\ell\,(\ell+1)}}{r}\left(\partial_r\xi_\Omega + \xi_r - \frac{2}{r}\xi_\Omega\right)\boldsymbol{b} + \sqrt{2(\ell+1)\ell}\,\partial_t\xi_{\rm ax}\boldsymbol{c}^0 \\
& - i\sqrt{2(\ell+1)\ell}\left(\partial_r\xi_{\rm ax} - \frac{\xi_{\rm ax}}{r}\right)\boldsymbol{c} + i\frac{\sqrt{2\,(\ell+2)\,(\ell+1)\,(\ell-1)}}{r}\xi_{\rm ax}\boldsymbol{d} + \frac{\sqrt{2\,(\ell+2)\,(\ell+1)\,\ell\,(\ell-1)}}{r^2}\xi_\Omega\boldsymbol{f} \\
& + \frac{\sqrt{2}}{r^2}\left(2rB\xi_r - \ell\,(\ell+1)\,\xi_\Omega\right)\boldsymbol{g}\,,
\end{aligned}
\tag{21}
$$

where the prime denotes a derivative with respect to r and, henceforth, we omit the (ℓ, m) indices to avoid cluttering. If we pick ξ^μ judiciously, we can eliminate one component of the metric perturbations in the axial sector and three in the polar sector.

We will adopt the *Regge-Wheeler* gauge, which is fixed by setting to zero all terms involving angular derivatives of the highest order [59, 60]

$$
h_2 = h_0^{(e)} = h_1^{(e)} = G = 0\,. \tag{22}
$$

However, for $\ell \leq 1$ this choice does not completely fix the gauge, because some of the tensor spherical harmonics are identically zero: more precisely, $\boldsymbol{b}^0 = \boldsymbol{b} = \boldsymbol{c}^0 = \boldsymbol{c} = 0$ for $\ell = 0$, and $\boldsymbol{d} = \boldsymbol{f} = 0$ for $\ell \leq 1$. This additional gauge freedom allows us to set one more perturbation function to 0. We choose

$$
\text{for } \ell = 1 \quad , \quad K = 0\,. \tag{23}
$$

The $\ell \leq 1$ modes do not contribute to the radiative degrees of freedom of the gravitational field, and in vacuum can be removed by a gauge transformation [60, 61]. However, in the presence of an environment (even if just a point-particle), they cannot be completely removed and carry physical significance through the matter sector. For our bosonic configuratons in particular, there will be dipolar scalar depletion.

2.3.3 Evolution Equations

We now have all the necessary machinery to tackle the linearized Einstein equations and obtain a set of ordinary differential equations (ODEs) for the perturbations. We will focus on the polar sector, because it is the one more technically involved and it dominates energy emission for (quasi-)circular motion (if you understand the polar sector, I am sure you can work out the axial sector by yourself). Our goal is to manipulate the perturbed Einstein-Klein Gordon system and find a system of 5 coupled ODEs that can be written schematically as

$$
\frac{d\vec{\mathcal{X}}}{dr} + \hat{\alpha}\vec{\mathcal{X}} = \vec{\mathcal{S}}\,, \tag{24}
$$

where $\vec{\mathcal{X}} = (H_0,\, H_1,\, K,\, \delta\Psi_+,\, \delta\Psi_-)$ and $\vec{\mathcal{S}}$ are the source terms directly related to the point particle.

Exercise. Reproduce the next computations for the $\ell \geq 2$ modes

- The $\theta\varphi$-component of Einstein's equations gives an algebraic relation between H_2 and H_0

$$
H_2 = H_0 - \frac{8\sqrt{2}\pi\, r^2}{\sqrt{n(1+n)}}\mathcal{F} \tag{25}
$$

- The tr-component of Einstein's equations gives a 1st-order ODE for K

$$
\begin{aligned}
& K' + \left(\frac{2}{r} - \frac{A'}{A}\right)\frac{K}{2} = \frac{H_0}{r} + \frac{i}{\sigma}\left(\frac{n}{r^2} + \frac{B}{r^2} + \frac{B'}{r} + 4\pi V_0 - \frac{4\pi\omega^2}{A}\Psi_0^2 + 4\pi B\Psi_0'^2\right)H_1 \\
& - \frac{4\pi\omega}{\sigma r^2}\left(\Psi_0 + r\Psi_0'\right)\left(\delta\Psi_+ - \delta\Psi_-\right) - \frac{4\pi}{r}\Psi_0'\left(\delta\Psi_+ + \delta\Psi_-\right) + \frac{4\pi}{r}\frac{\omega}{\sigma}\Psi_0\left(\delta\Psi_+' - \delta\Psi_-'\right) - \frac{8\sqrt{2}\pi\, r}{\sqrt{n(1+n)}}\mathcal{F}\,.
\end{aligned}
\tag{26}
$$

- The $t\theta$-component of Einstein's equations gives a 1st-order ODE for H_1

$$H_1' + \left(\frac{B'}{B} + \frac{A'}{A}\right)\frac{H_1}{2} = -\frac{i\sigma}{B}H_0 - \frac{i\sigma}{B}K + \frac{i\sigma}{B}\frac{8\sqrt{2}\pi\, r^2}{\sqrt{n(1+n)}} + 8\pi i\frac{\omega}{rB}\Psi_0\left(\delta\Psi_+ - \delta\Psi_-\right) + \mathcal{F} + \frac{i}{B}\frac{8\pi r}{\sqrt{1+n}}\mathcal{B}_0\,. \tag{27}$$

- The $r\theta$-component of Einstein's equations gives a 1st-order ODE for H_0

$$\begin{aligned} H_0' + \left(\frac{A'}{A} - \frac{1}{r}\right)H_0 = &-\left(\frac{2}{r} - \frac{A'}{A}\right)\frac{K}{2} - \frac{4\pi\omega}{\sigma r^2}\left(\Psi_0 + r\Psi_0'\right)\left(\delta\Psi_+ - \delta\Psi_-\right) - \frac{4\pi}{r}\Psi_0'\left(\delta\Psi_+ + \delta\Psi_-\right) \\ &+ 4\pi\frac{\omega}{r\sigma}\Psi_0\left(\delta\Psi_+' - \delta\Psi_-'\right) + \frac{i}{Ar^2\sigma}\left(A(n+B) - r^2\sigma^2 + rAB + 4\pi r^2 AV_0 - 4\pi r^2\omega^2\Psi_0^2 + 4\pi r^2 AB\Psi_0'^2\right)H_1 \\ &+ \frac{4\sqrt{2}\pi\, r^2}{\sqrt{n(1+n)}}\frac{A'}{A}\mathcal{F}\,. \end{aligned} \tag{28}$$

We know that in GR the gravitational field has only two degrees of freedom, so the ODEs above cannot be all independent. In fact, the rr-component of Einstein's equations yields an algebraic relation between H_0, H_1 and K which we could use to reduce the 3 ODEs above to only two (2 1st order ODEs $\Rightarrow$ 2 boundary conditions to impose $\Rightarrow$ 2 degrees of freedom). In the MATHEMATICA notebook, I chose to work with the 3 equations above, because it is more direct to input in the inhomogeneous part of the perturbed Klein-Gordon equation, which reads

$$\begin{aligned} &\delta\Psi_+'' + \frac{1}{2}\left(\frac{A'}{A} + \frac{B'}{B}\right)\delta\Psi_+' + \frac{1}{2r^2AB}\left(r\left(2r(\sigma+\omega)^2 - A'B\right) - A\left(4 + 4n + 2r^2U_0 + rB'\right)\right)\delta\Psi_+ - \frac{r\Psi_0}{B}\delta U \\ &- \frac{r\omega\sigma}{AB}\Psi_0 K + i\frac{r\omega}{B}\Psi_0 H_1' + r\Psi_0'(H_0' - K') + \frac{i}{2A^2B}\left(\Psi_0\left(rAB' + B(4A - rA')\right) + \Psi_0' 2r(\sigma+2\omega)AB\right)H_1 \\ &+ \frac{1}{2AB}\left(-2r\omega\left(\sigma+\omega\right)\Psi_0 + \left(rAB' + B\left(4A + rA'\right)\right)\Psi_0' + 2rAB\Psi_0''\right)H_0 - m_p\frac{4\sqrt{2}\pi r^3}{\sqrt{n(1+n)}}\Psi_0'\mathcal{F}' \\ &+ m_p\frac{4\sqrt{2}\pi r^2}{\sqrt{n(1+n)}AB}\left(r\sigma\omega\Psi_0 - \left(6AB + rA'B + rA'B\right)\Psi_0' - 2rAB\Psi_0''\right)\mathcal{F}\,. \end{aligned} \tag{29}$$

and the same equation for $\delta\Psi_-$ but with $\omega \to -\omega$.

Similar steps can be repeated for the $\ell = 1$ mode, where we also impose $K = 0$ to fix the additional gauge freedom. We leave this derivation for the notebook.

2.3.4 Zerilli master variable

At this stage, you are probably looking to the equations we have just written and thinking *"uff...this looks ugly..."*, specially if you have already had contact with BH perturbation theory and are familiar with the *Zerilli* master function [60, 62, 63].

Exercise. Check that for $\ell \geq 2$ and in a Schwarzschild background, where the background metric functions are

$$A(r) = B(r) = 1 - \frac{2M}{r} \quad , \quad \frac{dr_*}{dr} = \frac{1}{\sqrt{AB}} = \frac{1}{1 - 2M/r}\,, \tag{30}$$

the set of ODEs governing the gravitational perturbations we wrote above are equivalent to the single master equation for the Zerilli function Z

$$\frac{dZ^2}{dr_*^2} + \left(\sigma^2 - V_Z\right)Z = S_Z\,, \tag{31}$$

with the potential

$$V_Z = \frac{2\left(1 - 2M/r\right)}{r^3}\frac{9M^3 + 3n^2Mr^2 + n^2(1+n)r^3 + 9M^2nr}{(3M + \sigma r)}^2\,, \tag{32}$$

and the relation with the original variables being for example in Eqs. (17)-(19) of Ref. [64]. Here we report only the relation for K because it will prove useful below

$$K = \frac{dZ}{dr_*} + \frac{6M^2 + n(1+n)r^2 + 3Mnr}{r^2\left(3M + nr\right)}Z\,. \tag{33}$$

The Zerilli master function is a complex-valued gauge-invariant scalar which – as we will make explicit below – controls the radiative degrees of freedom of the gravitational field. For the axial sector there is an equivalent master wave equation for the *Regge-Wheeler* variable. This is definitely a much more elegant solution to the vacuum problem than solving a system of coupled ODEs. Unfortunately, in the presence of matter we do not have a notion of a master variable for the polar sector, although I personally believe there should be one with a more complicated dependence with respect to the original variables. There is ongoing work on this problem and hopefully in the near future we will have a master wave equation for generic (spherically-symmetric) spacetimes.

2.3.5 Boundary Conditions

The only ingredient we are missing to solve our evolution equations is to impose boundary conditions at the horizon and at infinity. For $\ell \geq 2$, all gravitational perturbations, which we denote by X, admit wave-like solutions ingoing at the horizon and outgoing at large radius. Since our numerical solver does not extend exactly to these radii, we impose a series expansion of the form [48, 65]

$$X\left(r\to\infty\right) = e^{+i\sigma r_*}\sum_{j=0}^{n_\infty}\frac{X_\infty^{(j)}}{r^j} \quad , \quad X\left(r\to 2M\right) = e^{-i\sigma r_*}\sum_{j=0}^{n_H} X_H^{(j)}\left(r-2M\right)^j \, , \tag{34}$$

where the coefficients $X^{(j)}_{\infty,H}$ are obtained by inserting these expansions in the homogeneous equations and solving them at each order in $(r-2M)$ and $1/r$, and set one of the 0-th coefficient to 1. In the notebook I only went to the 1-st order coefficient ($n_\infty = n_H = 1$), but adding more terms will make the results more precise. For $\ell = 1$ it is enough to set all gravitational perturbations to 0 at the horizon. In fact, in vacuum it is possible to find analytical solutions for them which in the Newtonian limit represent a fictitious force due to the fact that our reference frame centered at the primary BH is a non-inertial one [60, 63].

For the scalar perturbations, we also impose ingoing waves at the horizon and outgoing/regularity conditions at large distances. Because the field has a mass, the series expansions become [48, 65]

$$\delta\Psi_\pm\left(r\to\infty\right) = e^{+ik_\pm r_*} r^{-\nu_+}\sum_{j=0}^{n_\infty}\frac{\delta\Psi^{(j)}_{\pm,\infty}}{r^j} \quad , \quad \delta\Psi_\pm\left(r\to 2M\right) = e^{-i\omega_\pm r_*}\sum_{j=0}^{n_H}\delta\Psi^{(j)}_{\pm,H}\left(r-2M\right)^j \, , \tag{35}$$

where

$$\omega_\pm = \sigma \pm \omega \quad , \quad k_\pm = \text{sign}(\omega_\pm)\sqrt{\omega_\pm^2-\mu^2} \quad , \quad \nu_+ = -iM\mu^2/k_\pm \, . \tag{36}$$

We observe that only for frequencies $\omega_\pm > \mu$ there is emisson to infinity. For smaller frequencies, the energy that is transferred from the binary to the environment is not sufficient to surpass the binding energy of the scalar configuration and perturbations are confined, decaying exponentially at large distances.

2.3.6 Energy Fluxes and Orbital evolution

Once we solve the evolution equations we have all the necessary information to compute, up to order $\mathcal{O}(\epsilon^2)$, the fluxes of gravitational and scalar energy carried away to infinity and absorbed by the central BH. Generically, we can write them as

$$\dot{E}^S_L = -\sigma_L \lim_{r\to r_L} r^2 \int d\Omega \, T^S_{\mu\nu}\, \xi^\mu_{(t)}\, n^\nu_L \, , \tag{37}$$

where

$$S = \{\Psi, g\} \quad , \quad L = \{H, \infty\} \quad , \quad \sigma_{\{H,\infty\}} = -, + \quad , \quad \xi_{(t)} = \frac{\partial}{\partial t} \quad , \tag{38}$$

with S being the sector (scalar or gravitational), L the location (horizon or infinity), $\xi_{(t)}$ the Killing vector field associated to invariance under time translations and n^ν_L a normal vector to the respective hypersurface. For the scalar sector, the energy-momentum is the one in Eq. (4) and for the gravitational one we use Isaacson's effective energy-momentum tensor

$$T^g_{\mu\nu} = \frac{1}{64\pi}\left\langle \nabla_\mu \delta g^{\alpha\beta} \nabla_\nu \delta g_{\alpha\beta} \right\rangle \, . \tag{39}$$

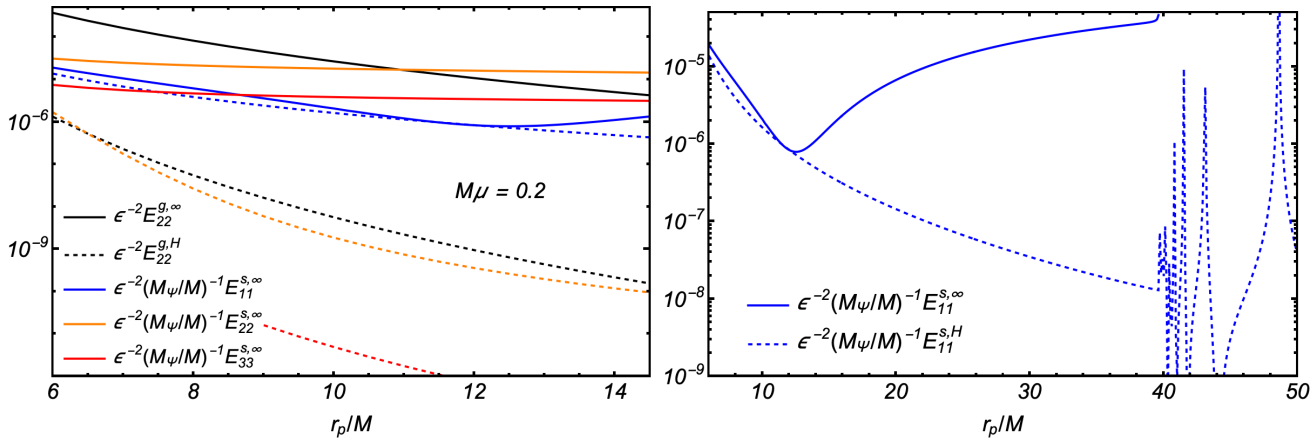

Figure 1: *Left Panel:* Scalar (s)/gravitational (g) energy fluxes at infinity (∞)/horizon (H) as a function of the orbital radius for a circular EMRI immersed in a spherical boson cloud with $M\mu = 0.2$; *Right Panel*: dipolar scalar flux for larger orbital separation.

One can show that in a vacuum background (which is the one we are going to use in the next section), the (time-averaged) gravitational flux can be written in terms of the Zerilli master function as [66]

$$\dot{E}^{g}_{\infty,H} = \lim_{r\to\infty,\,2M} \frac{1}{64\pi} \sum_{\ell,m} \frac{(\ell+2)!}{(\ell-2)!}\, \sigma^2\, |Z|^2 \,. \tag{40}$$

Using the relation in Eq. (33) (and its respective asymptotic limit for $r \to \infty$ and $r \to 2M$) we can rewrite these as

$$\dot{E}^{g}_{\infty} = \lim_{r\to\infty} \frac{1}{64\pi} \sum_{\ell,m} \frac{(\ell+2)!}{(\ell-2)!}\, |K|^2 \quad , \quad \dot{E}^{g}_{H} = \lim_{r\to 2M} \frac{1}{64\pi} \sum_{\ell,m} \frac{(\ell+2)!}{(\ell-2)!} \left| \frac{4M\,K}{\ell(\ell+1) - i\sigma 4M} \right|^2 , \tag{41}$$

Exercise. Using the asymptotic behavior dictated by the boundary conditions in Eqs. (35) show that the (time-averaged) scalar fluxes can be written as

$$\dot{E}^{\Psi}_{\infty} = \lim_{r\to\infty} \sum_{\ell,m} \omega_+ \,\mathrm{Re}(k_+)\, |\delta\Psi_+|^2 \quad , \quad \dot{E}^{\Psi}_{H} = \lim_{r\to 2M} \sum_{\ell,m} \omega_+^2\, |\delta\Psi_+|^2 \quad . \tag{42}$$

To compute the orbital backreaction due to this emission of energy, we still need to account for the depletion of the cloud itself. Under our assumptions ($\mathrm{Im}(\omega) = 0$ and no accretion onto the secondary), the mass M_Ψ of the bosonic configuration is related to its Noether charge via (check Appendix of Ref. [48])

$$M_\Psi = \omega Q \,, \tag{43}$$

and therefore under an adiabatic evolution

$$\dot{M}_\Psi = \omega \dot{Q} \,. \tag{44}$$

Exercise. Again using the asymptotic behavior of the scalar perturbations (and the fact that the Noether current is conserved) show that

$$\dot{Q}_{\infty} = \lim_{r\to\infty} \mathrm{Re}(k_+)\, |\delta\Psi_+|^2 \quad , \quad \dot{Q}_{H} = \lim_{r\to 2M} \omega_+\, |\delta\Psi_+|^2 \,. \tag{45}$$

With this we can finally write a balance law for the adiabatic evolution of the orbital energy of the particle

$$\frac{dE_p}{dt} = -\dot{E}^{g}_{\infty} - \dot{E}^{g}_{H} - (\dot{E}^{\Psi}_{\infty} - \omega\dot{Q}_{\infty}) - (\dot{E}^{\Psi}_{H} - \omega\dot{Q}_{H}) \,. \tag{46}$$

3 Results

3.1 Spherical Bosonic Clouds

We have all the machinery prepared so let us apply it to a particular system. We are going to do it for the simplest system we can think of which are spherical (ground-state) boson clouds [25]. These are (nodless) solutions for Einstein-Klein-Gordon system in the test-field limit, where even the backreaction of the

background field $\hat{\Psi}$ on the background geometry is neglected, and the metric reduces to Schwarzschild (30). In this limit, the bosonic cloud has a structure similar to the hydrogen with $\alpha = M\mu$ playing the role of a *gravitational fine-structure constant* [30]. For $M\mu \ll 1$ they also admit approximate analytical descriptions in terms of Laguerre polynomials, and for the spherical setup in particular [25]

$$\Psi_0(r) \approx \sqrt{\frac{M_\Psi}{\pi M_{\rm BH}}}(M_{\rm BH}\mu)^2 \left(1-\frac{2M_{\rm BH}}{r}\right)^{-2i\mu M_{\rm BH}} e^{-M_{\rm BH}\mu^2 r} \quad , \quad \omega = \mu\left[1-\frac{1}{2}\left(M\mu\right)^2\right] . \tag{47}$$

To be fully consistent with the test-field approximation we will neglect all terms related with the scalar field in the gravitational sector of the evolution equations. This is therefore equivalent to solving the vacuum gravitational problem and then using those perturbations as a source of the Klein-Gordon equation. For this it would therefore have been more practical to work with the Zerilli master function and reconstruct the metric from it. However, with an eye on the generalization for when the test field approximation is not possible, in the MATHEMATICA notebook I still opted to work directly with the set of 5 ODEs.

I will leave details on the numerical implementation for the notebook, and simply jump to the numerical results. In Fig. 1 (left panel), we compare the scalar energy flux carried by different multipoles with the dominant quadrupolar gravitational flux as a function of the orbital radius of the secondar. My solver is not efficient enough and so I was not able to probe very large radius for all the multipoles. However, it is clear that at larger radius the scalar flux can compete with gravitational radiation. We only show values for one value of μ, but we note there is *no* known an analytical scaling of fluxes with μ. This is more challenging from the modelling perspective but should benefit the detection of these effects, since typically such behavior helps breaking degeneracies in the parameter space.

In the right panel we show the dipolar fluxes for larger orbital separations, which is enough to discuss the essential phenomenology of this system. We observe very distinctive features... let us try to understand them.

3.2 A gravitational atom: analogy with Quantum Mechanics

We have discussed that superradiant clouds have a structure similar to the hydrogen atom, which has been deeply explored in Refs [52–55]. We are now going to make use of this analogy to interpret our results.

A flux of energy arriving to infinity should correspond to scalar particles escaping the potential well of the bosonic cloud and being ejected from it. In the hydrogen atom, this would correspond to its *ionization* with the ejection of the electron (the fact that in the hydrogen atom we only have 1 particle is what makes the system *quantum*). From the *photoelectric effect* we know that emission is not continuous with respect to the intensity of the external radiation. Instead, light has to have frequency high enough the exceed the binding energy of the electron to the nuclei. Our system follows the same trend. The energy being imparted from the binary to the cloud has to exceed a certain treshold, $m\Omega_p > \mu - \omega$, in order to activate cloud ionization and emission of scalar radiation to infinity. That is why we see a discontinuity in Fig. 1 for the dipolar flux at $r_p \approx 39.6M$, which corresponds to a frequency $\Omega_p = \sqrt{M/r_p^3} \approx 4.01 \times 10^{-3}$, while $\mu - \omega = 4 \times 10^{-3}$. All modes will have this discontinuity at a radius corresponding to a frequency $(\mu-\omega)/m$, so the larger the radius, the larger the mode that dominates scalar energy emission.

Moving to the flux at the horizon, we need to understand those peaks. Our cloud is in the *fundamental* mode of a spherically symmetric configuration, i.e. the $\ell = m = 0$ mode with the lowest energy. But there are *overtones* corresponding to excited, higher-energy, spherically-symmetric states. If we were to consider non-spherical clouds, then again in analogy with the hydrogen atom there will be an energy splitting between modes with different angular momentum (labelled by ℓ, m) [25]

$$\omega_{n\ell m} = \mu\left(1-\frac{\alpha^2}{2n^2}-\frac{\alpha^4}{8n^4}-\frac{(3n-2\ell_i-1)\,\alpha^4}{n^4(\ell_i+1/2)}+\frac{2(a/M)m_i\alpha^5}{n^3\ell_i(\ell_i+1)(\ell_i+1/2)}+\mathcal{O}(\alpha^6)\right) , \tag{48}$$

where $n = 1, 2, ...$ labels the overtone and we also included the *hyperfine* splitting ($\Delta m \neq 0$) when the BH is rotating ($a \neq 0$) [55]. If the binary has orbital frequency equal to the energy difference between two states, then it can induce resonant transitions between them. Those are precisely the peaks we are observing. The binary is transferring energy to the cloud and inducing resonant transitions from the fundamental $n = 1$, $\ell = m = 0$ to higher overtones, which decay much faster than the fundamental one and are quickly absorbed by the primary BH.

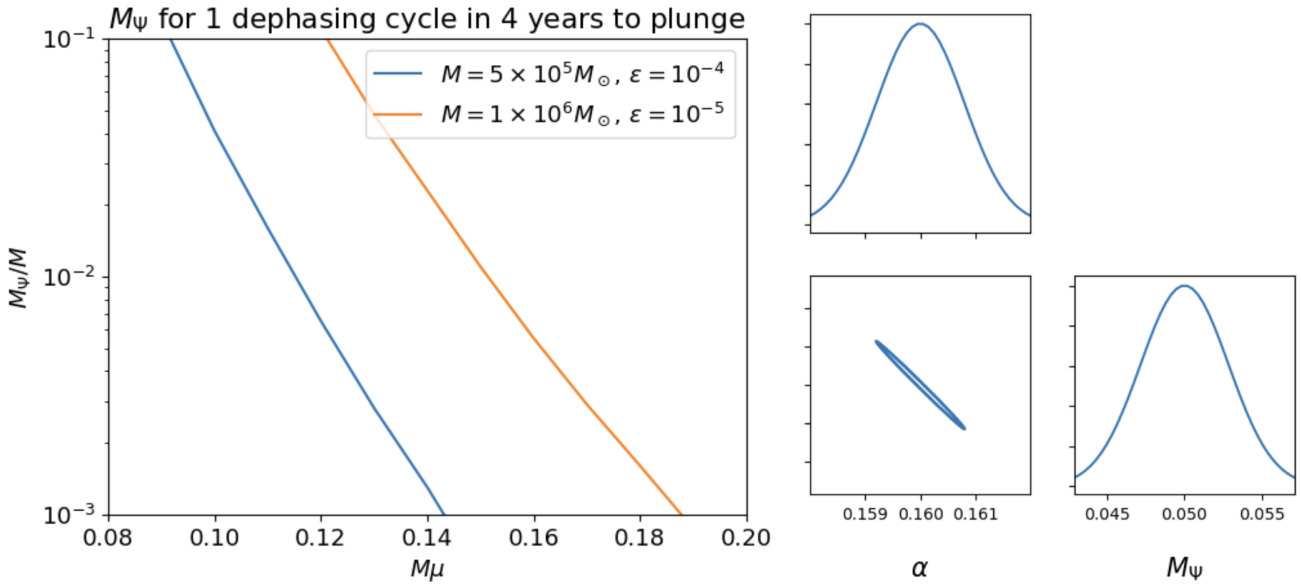

Figure 2: *Left Panel*: Minimum mass M_Ψ which for a fixed μ yields 1 cycle of dephasing after 4 years of observation that ends in a plunge, for two different EMRIs in prograde orbits immersed in a $\ell = m = 1$ cloud (non-spherical, using results from Ref. [48]) *Right Panel*: Marginalized posterior of the cloud parameters for an EMRI with $M = 4\times10^5\, M\odot$, $\epsilon = 10^{-4}$, observed with LISA 4 years prior to plunge (initial radius is $r_p^i = 19.945M$, the spin of the central BH is $a/M = 0.6$, and the signal-to-noise ratio is SNR = 50). Results are obtained using the FastEMRIWaveform package [67–69] and a Fisher-Matrix formalism.

3.3 LISA Forecasts (work-in-progress)

What are then the consequences of our results to GW astronomy, in particular to LISA? The interaction of the binary with the environment makes it lose energy at a different rate, which alters its trajectory. This has direct impact on the phase of the GW signal emitted by the EMRI

$$\phi_{\rm GW} = 2\int_{T_{\rm f}-T_{\rm obs}}^{T_{\rm f}} \Omega_p(t)dt = 2\int_{T_{\rm f}-T_{\rm obs}}^{T_{\rm f}} \frac{d\varphi(t)}{dt}dt = 2\int_{T_{\rm f}-T_{\rm obs}}^{T_{\rm f}} \left(\frac{d\varphi}{dr}\right)\left(\frac{dr}{dE}\right)\left(\frac{dE(t)}{dt}\right)dt\,, \tag{49}$$

which we can measure very accurately. How large a dephasing needs to be to be measurable depends on different aspects, namely the signal-to-noise ratio (how "loud" the GW signal is with respect to the noise power), but a 1 cycle dephasing is a criteria often used for detectability (though not a sufficient one [70]).

In the left panel of Fig. 2 we show, for a given value of $M\mu$, the minimum mass of the bosonic cloud that leads to 1 dephasing cycle after 4 years of observation – the duration of the LISA mission – that end in a plunge, for two different EMRIs (for this I use the results for non-spherical clouds from Ref. [48] for prograde orbits around a $\ell = m = 1$ cloud). Considering superradiant clouds can be as massive as $M_\Psi \sim 0.1M$, we conclude there is an astrophysically relevant region of the parameter space that could lead to measurable effects. For the system with larger mass ratio ($\epsilon = 10^{-4}$), the minimum mass is smaller because the initial separation is larger, $r_p^i \sim 20M$ *vs* $r_p^i \sim 10M$ for the system with smaller mass-ratio ($\epsilon = 10^{-5}$). For larger radius, the relative ratio between the scalar and gravitational flux is larger and hence the effect of the cloud is more significant. Note that for these inspirals we do not hit any resonance, for which the orbital backreaction becomes more involved, since the adiabaticity assumption breaks down [55].

To validate this expectation, we implemented our results in the state-of-the-art FastEMRIWaveform package [67–69]. This a modular Python code to which the user can easily add corrections to the inspiral in form of energy fluxes, as is the case of our EMRI in a bosonic cloud, and compute the respective waveform assuming a Kerr background. Using this waveform, we performed parameter estimation for LISA using a Fisher Matrix formalism [71–73] [1]. We display results in the right panel of Fig. 2, for a $\ell = m = 1$ cloud with $M\mu = 0.16$ and $M_\Psi = 0.05$, and the EMRI with $M = 4\times10^5\, M\odot$, $\epsilon = 10^{-4}$, $a/M = 0.6$ (spin at which the superradiant instability saturates for this boson mass), initial radius $r_p^i = 19.945M$, and a signal-to-noise-ratio of SNR = 50. The parameters of the cloud can be recovered with relative error $\lesssim 10\%$, while the recovery of the vacuum GR binary parameters is not deteriorated. The prospects for probing ultralight fields with EMRIs are very exciting!

[1] The technicalities behind this would require 2 more hours to explain...

4 Discussion

We have focused on the most simple system possible for the theory we considered: a circular inspiral around a non-rotating BH surrounded by a spherical scalar cloud. We will end by discussing how to extend our results to more complicated scenarios and what are the possible directions to pursue in this research programme. All the topics below are certainly paper-worthy (some of them which have already been written or are in the making process).

Non-spherical clouds: The first extension to consider are non-spherical clouds, which were studied in Ref. [48]. They are better motivated astrophysically through superradiance, though we should note spherical structures can be formed via other mechanisms, like accretion [44, 74, 75] or dynamical capture from a DM halo [76]. For non-spherical clouds, the technical setup is almost the same as what we did, with the only difference appearing in the non-homogeneous part (source term) of the Klein-Gordon equation. Essentially, since the cloud is non-spherical, the source term with angular index $\{\ell_s, m_s\}$ can induce the transition between states $\{\ell_i,\, m_i\} \to \{\ell_f,\, m_f\}$. Formally, this shows up as integrals of the type

$$\mathcal{P}^{\ell_i,\ell_s,\ell_f}_{m_i,m_s,m_f} = \int d\Omega Y^*_{\ell_f m_f} Y_{\ell_s m_s} Y_{\ell_i m_i}\,. \tag{50}$$

These integrals are only non-zero for particular combinations of $\{\ell_f,\, \ell_s,\, \ell_i\}$ and $\{m_f,\, m_s,\, m_i\}$ which define a set of transition rules between states (very reminiscent of the Clebsch-Gordan coefficients/Wigner 3-j symbols).

Rotating configurations: rotation of the central BH is also a necessary ingredient in superradiance. For a rotating background vacuum spacetime, it is still possible to write a master wave equation for the radiative degrees freedom, known as the Teukolsky equation [77]. However, the metric reconstruction that is necessary to input in the source term of the Klein-Gordon equation becomes extremely more involved [78]. Another route is to consider a slowly-rotating approximation for the background, in which the structure of the equations is more similar to what we have employed [79]. This strategy looks particularly useful to handle superradiant clouds since when their growth saturates, at $M\Omega_H \sim M\mu$, the BH spin is far from extremality [29].

Fuzzy DM Solitions: In the beginning of our discussion, we mentioned ultralight fields can also form self-gravitating structures – boson stars or fuzzy soliton – which may describe the inner core of DM halos. Even if parasited by a BH at their centre, these structures can be stable over timescales larger than the age of the Universe [44]. It is therefore natural to also consider an EMRI evolving immersed in a fuzzy DM soliton, a problem which has been studied in Ref. [49] (under numerous approximations). The main technical complication in this is precisely that the self-gravity of the scalar configuration is non-negligible, so the background spacetime cannot be approximated to be pure vacuum (i.e. Schwarzschild) and, *a priori*, the gravitational sector does not decouple from the scalar one. In other words, one needs to solve the coupled system of 5 ODEs at the same time. A thorough exploration of the parameter space for these systems remains to be done.

Eccentric/Inclined orbits: Throughout our analysis we have assumed the EMRI exists but we have ignored its past history and the impact the EMRI's formation channel has on the configuration of the binary (i.e. its eccentricity and inclination) and the state of the cloud. The most "standard" mechanism for EMRI formation in vacuum is multi-body scattering in dense stellar clusters where one body is launched to the central SMBH in an almost-plunging highly eccentric orbit ($e \gtrsim 0.999$), which then circularizes via GW emission, and may enter the LISA band still at moderate eccentricity ($e \lesssim 0.7$) and arbitrary inclination [1]. EMRI formation in non-vacuum astrophysical environments is still poorly understood, but recent results in the context of accretion disks indicate the interaction of the small compact body with the disk assists EMRI formation [80–82], albeit with residual eccentricity (but note these studies ignore important physics, namely stochastic variations in the body-disk interactions [83]). What about for EMRIs forming in supperadiant clouds? Ref. [55] has addressed this question and found two sounding phenomenological conclusions: first for most initial orbital configurations, the passage(s) through resonance(s) depletes the cloud almost entirely by the time the compact binary enters the frequency band of GW detectors. The cloud has the highest chance of survival for retrograde orbits (with respect to the BH spin); in any case, resonances leave distinctive features in eccentricity and inclination, with the authors reporting the existence of fixed points in the trajectory evolution of these quantities (this has also been observed in GRMHD simulations of binaries in accretion disks [84]). Extending our study to generic ones appears therefore of great relevance.

Real/Vector fields: another possible extension is to consider other type of ultralight fields. For example, we could have studied *real* scalar fields instead of complex ones. For the former, the energy-momentum tensor is no longer time-independent – there is no equivalent of the Noether charge in Eq. (2) – and the cloud will source GWs. The main technical difference would be then to consider this energy loss in the balance law we wrote for the binary's inspiral. Other possibility is to consider vector fields, for which the superradiant instability is actually stronger. Here, we would need to substitute the Klein-Gordon equation by the Proca equation for the ultralight vector field $\boldsymbol{A}$

$$\nabla_\mu \left(\partial^\mu A^\nu - \partial^\nu A^\mu\right) = \mu^2 A^\nu \,, \tag{51}$$

but the rest of the logical steps would be the same.

Environmental Self-Force: this is more like an entire career research programme rather than a self-contained project. In the end, the problem that we are trying to solve is some kind of *perturbative non-vacuum two-body problem*. In the extreme-mass-ratio limit, a proper solution to this would correspond to a self-force theory that includes environmental effects. Let us remark that vacuum self-force is already an extremely challenging and technical problem and there is a whole decade of necessary work to complete by the time LISA flies for us to be able to do science with EMRIs. In any case, we may hypothesise how an environmental self-force theory would look like. As we mentioned already, a key property of the self-force program is that the orbital phase evolves on a timescale $T_o \sim M$ which is much faster than the inspiral timescale dictated by GW emission $T_i \sim M^2/m_p$, which allows to separate the phase from the orbital evolution via a *two-timescale* expansion [4, 58]. In the presence of an environment, there will corrections to these timescales which for a compact binary should typically scale with the central energy density $M^2\rho_c$ of the matter distribution. One could then envision some kind of *three-timescale* expansion for this problem. This might sound crazy but it is not unheard of in Physics. A quick Google search led me to a three-timescale approximate solution to the damped harmonic oscillator [85], to the Van der Pol oscillator, and to neutron kinetics in nuclear reactors [86].

With this discussion I hope to have convinced you that there are multiple interesting open problems in this research field which cover a broad range of techniques that go from formal/theoretical tasks to more observational ones. Working in fundamental fields is really working in the intersection of strong-field gravity, particle physics, and astrophysics and if some of these problems excite you there are many people around the school/workshop you can talk to.

References

[1] Stanislav Babak, Jonathan Gair, Alberto Sesana, Enrico Barausse, Carlos F. Sopuerta, Christopher P. L. Berry, Emanuele Berti, Pau Amaro-Seoane, Antoine Petiteau, and Antoine Klein. Science with the space-based interferometer LISA. V: Extreme mass-ratio inspirals. *Phys. Rev.*, D95(10):103012, 2017.

[2] John Kormendy and Luis C. Ho. Coevolution (or not) of supermassive black holes and host galaxies. *Annual Review of Astronomy and Astrophysics*, 51(1):511–653, August 2013.

[3] Monica Colpi et al. LISA Definition Study Report. 2 2024.

[4] Tanja Hinderer and Eanna E. Flanagan. Two timescale analysis of extreme mass ratio inspirals in Kerr. I. Orbital Motion. *Phys. Rev. D*, 78:064028, 2008.

[5] Leor Barack et al. Black holes, gravitational waves and fundamental physics: a roadmap. *Class. Quant. Grav.*, 36(14):143001, 2019.

[6] Pau Amaro-Seoane et al. Astrophysics with the Laser Interferometer Space Antenna. *Living Rev. Rel.*, 26(1):2, 2023.

[7] Pierre Auclair et al. Cosmology with the Laser Interferometer Space Antenna. *Living Rev. Rel.*, 26(1):5, 2023.

[8] K. G. Arun et al. New horizons for fundamental physics with LISA. *Living Rev. Rel.*, 25(1):4, 2022.

[9] R. et al. Abbott. Gwtc-3: Compact binary coalescences observed by ligo and virgo during the second part of the third observing run. *Phys. Rev. X*, 13:041039, Dec 2023.

[10] Scott A. Hughes, Niels Warburton, Gaurav Khanna, Alvin J. K. Chua, and Michael L. Katz. Adiabatic waveforms for extreme mass-ratio inspirals via multivoice decomposition in time and frequency. *Phys. Rev. D*, 103(10):104014, 2021. [Erratum: Phys.Rev.D 107, 089901 (2023)].

[11] Barry Wardell, Adam Pound, Niels Warburton, Jeremy Miller, Leanne Durkan, and Alexandre Le Tiec. Gravitational Waveforms for Compact Binaries from Second-Order Self-Force Theory. *Phys. Rev. Lett.*, 130(24):241402, 2023.

[12] Nikolas A. Wittek et al. Worldtube excision method for intermediate-mass-ratio inspirals: Scalar-field model in 3+1 dimensions. *Phys. Rev. D*, 108(2):024041, 2023.

[13] Adam Pound and Barry Wardell. Black hole perturbation theory and gravitational self-force. 1 2021.

[14] Leor Barack and Adam Pound. Self-force and radiation reaction in general relativity. *Rept. Prog. Phys.*, 82(1):016904, 2019.

[15] R. D. Peccei and Helen R. Quinn. CP conservation in the presence of pseudoparticles. *Phys. Rev. Lett.*, 38:1440–1443, Jun 1977.

[16] Steven Weinberg. A new light boson? *Phys. Rev. Lett.*, 40:223–226, Jan 1978.

[17] Asimina Arvanitaki, Savas Dimopoulos, Sergei Dubovsky, Nemanja Kaloper, and John March-Russell. String Axiverse. *Phys. Rev. D*, 81:123530, 2010.

[18] Lam Hui, Jeremiah P. Ostriker, Scott Tremaine, and Edward Witten. Ultralight scalars as cosmological dark matter. *Phys. Rev. D*, 95(4):043541, 2017.

[19] Lam Hui. Wave Dark Matter. *Ann. Rev. Astron. Astrophys.*, 59:247–289, 2021.

[20] M. Iu. Khlopov, B. A. Malomed, and Ia. B. Zeldovich. Gravitational instability of scalar fields and formation of primordial black holes. *Monthly Notices of the Royal Astronomical Society*, 215:575–589, August 1985.

[21] William H. Press and Saul A. Teukolsky. Floating Orbits, Superradiant Scattering and the Black-hole Bomb. , 238(5361):211–212, July 1972.

[22] Sam R. Dolan. Instability of the massive Klein-Gordon field on the Kerr spacetime. *Phys. Rev. D*, 76:084001, 2007.

[23] William E. East and Frans Pretorius. Superradiant Instability and Backreaction of Massive Vector Fields around Kerr Black Holes. *Phys. Rev. Lett.*, 119(4):041101, 2017.

[24] William E. East. Massive Boson Superradiant Instability of Black Holes: Nonlinear Growth, Saturation, and Gravitational Radiation. *Phys. Rev. Lett.*, 121(13):131104, 2018.

[25] Richard Brito, Vitor Cardoso, and Paolo Pani. Superradiance. *Lect. Notes Phys.*, 906:pp.1–237, 2015.

[26] Steven L. Detweiler. KLEIN-GORDON EQUATION AND ROTATING BLACK HOLES. *Phys. Rev. D*, 22:2323–2326, 1980.

[27] Vitor Cardoso and Shijun Yoshida. Superradiant instabilities of rotating black branes and strings. *JHEP*, 07:009, 2005.

[28] Asimina Arvanitaki and Sergei Dubovsky. Exploring the String Axiverse with Precision Black Hole Physics. *Phys. Rev. D*, 83:044026, 2011.

[29] Richard Brito, Vitor Cardoso, and Paolo Pani. Black holes as particle detectors: evolution of superradiant instabilities. *Class. Quant. Grav.*, 32(13):134001, 2015.

[30] Daniel Baumann, Horng Sheng Chia, John Stout, and Lotte ter Haar. The Spectra of Gravitational Atoms. *JCAP*, 12:006, 2019.

[31] Richard Brito, Shrobana Ghosh, Enrico Barausse, Emanuele Berti, Vitor Cardoso, Irina Dvorkin, Antoine Klein, and Paolo Pani. Stochastic and resolvable gravitational waves from ultralight bosons. *Phys. Rev. Lett.*, 119(13):131101, 2017.

[32] Richard Brito, Shrobana Ghosh, Enrico Barausse, Emanuele Berti, Vitor Cardoso, Irina Dvorkin, Antoine Klein, and Paolo Pani. Gravitational wave searches for ultralight bosons with LIGO and LISA. *Phys. Rev. D*, 96(6):064050, 2017.

[33] Maximiliano Isi, Ling Sun, Richard Brito, and Andrew Melatos. Directed searches for gravitational waves from ultralight bosons. *Phys. Rev. D*, 99(8):084042, 2019. [Erratum: Phys.Rev.D 102, 049901 (2020)].

[34] Chen Yuan, Richard Brito, and Vitor Cardoso. Probing ultralight dark matter with future ground-based gravitational-wave detectors. *Phys. Rev. D*, 104(4):044011, 2021.

[35] David J. Kaup. Klein-gordon geon. *Phys. Rev.*, 172:1331–1342, Aug 1968.

[36] Edward Seidel and Wai-Mo Suen. Formation of solitonic stars through gravitational cooling. *Phys. Rev. Lett.*, 72:2516–2519, 1994.

[37] Jae-weon Lee and In-gyu Koh. Galactic halos as boson stars. *Phys. Rev. D*, 53:2236–2239, 1996.

[38] Steven L. Liebling and Carlos Palenzuela. Dynamical Boson Stars. *Living Rev. Rel.*, 15:6, 2012.

[39] Diego F. Torres, S. Capozziello, and G. Lambiase. A Supermassive scalar star at the galactic center? *Phys. Rev. D*, 62:104012, 2000.

[40] Hsi-Yu Schive, Tzihong Chiueh, and Tom Broadhurst. Cosmic Structure as the Quantum Interference of a Coherent Dark Wave. *Nature Phys.*, 10:496–499, 2014.

[41] Hsi-Yu Schive, Ming-Hsuan Liao, Tak-Pong Woo, Shing-Kwong Wong, Tzihong Chiueh, Tom Broadhurst, and W. Y. Pauchy Hwang. Understanding the Core-Halo Relation of Quantum Wave Dark Matter from 3D Simulations. *Phys. Rev. Lett.*, 113(26):261302, 2014.

[42] Jan Veltmaat, Jens C. Niemeyer, and Bodo Schwabe. Formation and structure of ultralight bosonic dark matter halos. *Phys. Rev. D*, 98(4):043509, 2018.

[43] Juan Barranco, Argelia Bernal, Juan Carlos Degollado, Alberto Diez-Tejedor, Miguel Megevand, Dario Nunez, and Olivier Sarbach. Self-gravitating black hole scalar wigs. *Phys. Rev. D*, 96(2):024049, 2017.

[44] Vitor Cardoso, Taishi Ikeda, Rodrigo Vicente, and Miguel Zilhão. Parasitic black holes: The swallowing of a fuzzy dark matter soliton. *Phys. Rev. D*, 106(12):L121302, 2022.

[45] Ben Moore. Evidence against dissipation-less dark matter from observations of galaxy haloes. , 370(6491):629–631, August 1994.

[46] Julio F. Navarro, Carlos S. Frenk, and Simon D. M. White. A Universal density profile from hierarchical clustering. *Astrophys. J.*, 490:493–508, 1997.

[47] David H. Weinberg, James S. Bullock, Fabio Governato, Rachel Kuzio de Naray, and Annika H. G. Peter. Cold dark matter: controversies on small scales. *Proc. Nat. Acad. Sci.*, 112:12249–12255, 2015.

[48] Richard Brito and Shreya Shah. Extreme mass-ratio inspirals into black holes surrounded by scalar clouds. *Phys. Rev. D*, 108(8):084019, 2023.

[49] Francisco Duque, Caio F. B. Macedo, Rodrigo Vicente, and Vitor Cardoso. Axion Weak Leaks: extreme mass-ratio inspirals in ultra-light dark matter. 12 2023.

[50] Vitor Cardoso, Kyriakos Destounis, Francisco Duque, Rodrigo Panosso Macedo, and Andrea Maselli. Black holes in galaxies: Environmental impact on gravitational-wave generation and propagation. *Phys. Rev. D*, 105(6):L061501, 2022.

[51] Vitor Cardoso, Kyriakos Destounis, Francisco Duque, Rodrigo Panosso Macedo, and Andrea Maselli. Gravitational Waves from Extreme-Mass-Ratio Systems in Astrophysical Environments. *Phys. Rev. Lett.*, 129(24):241103, 2022.

[52] Daniel Baumann, Gianfranco Bertone, John Stout, and Giovanni Maria Tomaselli. Ionization of gravitational atoms. *Phys. Rev. D*, 105(11):115036, 2022.

[53] Daniel Baumann, Gianfranco Bertone, John Stout, and Giovanni Maria Tomaselli. Sharp Signals of Boson Clouds in Black Hole Binary Inspirals. *Phys. Rev. Lett.*, 128(22):221102, 2022.

[54] Giovanni Maria Tomaselli, Thomas F. M. Spieksma, and Gianfranco Bertone. Dynamical Friction in Gravitational Atoms. 5 2023.

[55] Giovanni Maria Tomaselli, Thomas F. M. Spieksma, and Gianfranco Bertone. The resonant history of gravitational atoms in black hole binaries. 3 2024.

[56] Norichika Sago, Hiroyuki Nakano, and Misao Sasaki. Gauge problem in the gravitational selfforce. 1. Harmonic gauge approach in the Schwarzschild background. *Phys. Rev. D*, 67:104017, 2003.

[57] Francisco Duque. *Gravitational Waves and the Galactic Potential*. PhD thesis, U. Lisbon (main), 2023.

[58] Jeremy Miller and Adam Pound. Two-timescale evolution of extreme-mass-ratio inspirals: waveform generation scheme for quasicircular orbits in Schwarzschild spacetime. *Phys. Rev. D*, 103(6):064048, 2021.

[59] Tullio Regge and John A. Wheeler. Stability of a Schwarzschild singularity. *Phys. Rev.*, 108:1063–1069, 1957.

[60] F. J. Zerilli. Gravitational field of a particle falling in a schwarzschild geometry analyzed in tensor harmonics. *Phys. Rev. D*, 2:2141–2160, 1970.

[61] Steven L. Detweiler and Eric Poisson. Low multipole contributions to the gravitational selfforce. *Phys. Rev. D*, 69:084019, 2004.

[62] Frank J. Zerilli. Effective potential for even parity Regge-Wheeler gravitational perturbation equations. *Phys. Rev. Lett.*, 24:737–738, 1970.

[63] Karl Martel and Eric Poisson. Gravitational perturbations of the Schwarzschild spacetime: A Practical covariant and gauge-invariant formalism. *Phys. Rev. D*, 71:104003, 2005.

[64] Emanuele Berti, Vitor Cardoso, and Andrei O. Starinets. Quasinormal modes of black holes and black branes. *Class. Quant. Grav.*, 26:163001, 2009.

[65] Caio F. B. Macedo, Paolo Pani, Vitor Cardoso, and Luís C. B. Crispino. Astrophysical signatures of boson stars: quasinormal modes and inspiral resonances. *Phys. Rev. D*, 88(6):064046, 2013.

[66] Karl Martel. Gravitational waveforms from a point particle orbiting a schwarzschild black hole. *Phys. Rev. D*, 69:044025, Feb 2004.

[67] Michael L. Katz, Alvin J. K. Chua, Niels Warburton, and Scott A. Hughes. BlackHolePerturbationToolkit/FastEMRIWaveforms: Official Release, August 2020.

[68] Alvin J. K. Chua, Michael L. Katz, Niels Warburton, and Scott A. Hughes. Rapid generation of fully relativistic extreme-mass-ratio-inspiral waveform templates for LISA data analysis. *Phys. Rev. Lett.*, 126(5):051102, 2021.

[69] Michael L. Katz, Alvin J. K. Chua, Lorenzo Speri, Niels Warburton, and Scott A. Hughes. Fast extreme-mass-ratio-inspiral waveforms: New tools for millihertz gravitational-wave data analysis. *Phys. Rev. D*, 104(6):064047, 2021.

[70] Ollie Burke, Gabriel Andres Piovano, Niels Warburton, Philip Lynch, Lorenzo Speri, Chris Kavanagh, Barry Wardell, Adam Pound, Leanne Durkan, and Jeremy Miller. Assessing the importance of first postadiabatic terms for small-mass-ratio binaries. *Phys. Rev. D*, 109(12):124048, 2024.

[71] Curt Cutler and Michele Vallisneri. LISA detections of massive black hole inspirals: Parameter extraction errors due to inaccurate template waveforms. *Phys. Rev. D*, 76:104018, 2007.

[72] Michele Vallisneri. Use and abuse of the Fisher information matrix in the assessment of gravitational-wave parameter-estimation prospects. *Phys. Rev. D*, 77:042001, 2008.

[73] Shubham Kejriwal, Lorenzo Speri, and Alvin J. K. Chua. Impact of Correlations on the Modeling and Inference of Beyond Vacuum-GR Effects in Extreme-Mass-Ratio Inspirals. 12 2023.

[74] Lam Hui, Daniel Kabat, Xinyu Li, Luca Santoni, and Sam S. C. Wong. Black Hole Hair from Scalar Dark Matter. *JCAP*, 06:038, 2019.

[75] Katy Clough, Pedro G. Ferreira, and Macarena Lagos. Growth of massive scalar hair around a Schwarzschild black hole. *Phys. Rev.*, D100(6):063014, 2019.

[76] Dmitry Budker, Joshua Eby, Marco Gorghetto, Minyuan Jiang, and Gilad Perez. A Generic Formation Mechanism of Ultralight Dark Matter Solar Halos. 6 2023.

[77] Saul A. Teukolsky. Perturbations of a Rotating Black Hole. I. Fundamental Equations for Gravitational, Electromagnetic, and Neutrino-Field Perturbations. , 185:635–648, October 1973.

[78] Stefan Hollands and Vahid Toomani. Metric Reconstruction in Kerr Spacetime. 5 2024.

[79] Paolo Pani, Emanuele Berti, and Leonardo Gualtieri. Scalar, Electromagnetic and Gravitational Perturbations of Kerr-Newman Black Holes in the Slow-Rotation Limit. *Phys. Rev. D*, 88:064048, 2013.

[80] Zhen Pan, Zhenwei Lyu, and Huan Yang. Wet extreme mass ratio inspirals may be more common for spaceborne gravitational wave detection. *Phys. Rev. D*, 104(6):063007, 2021.

[81] Zhen Pan and Huan Yang. Formation Rate of Extreme Mass Ratio Inspirals in Active Galactic Nuclei. *Phys. Rev. D*, 103(10):103018, 2021.

[82] Andrea Derdzinski and Lucio Mayer. In-situ extreme mass ratio inspirals via sub-parsec formation and migration of stars in thin, gravitationally unstable AGN discs. 5 2022.

[83] A. Derdzinski, D. D'Orazio, P. Duffell, Z. Haiman, and A. MacFadyen. Evolution of gas disc–embedded intermediate mass ratio inspirals in the $LISA$ band. *Mon. Not. Roy. Astron. Soc.*, 501(3):3540–3557, 2021.

[84] Alessia Franchini, Alessandra Prato, Cristiano Longarini, and Alberto Sesana. On the behaviour of eccentric sub-pc massive black hole binaries embedded in massive discs. 2 2024.

[85] Per Jakobsen. Introduction to the method of multiple scales. 12 2013.

[86] Bruno Merk and Dan Cacuci. Multiple timescale expansions for neutron kinetics - i: Illustrative application to the point-kinetics model. *Nuclear Science and Engineering - NUCL SCI ENG*, 151:184–193, 10 2005.